

## CT452/CT453 SLIT BUSBAR DESIGN

By Allegro MicroSystems

### ABSTRACT

This application note discusses the design and operational principle of a serpentine-style busbar. Air-gap spacing is the most critical parameter, followed by slit-to-slit distance, and finally the actual slit width.

### INTRODUCTION

The CT452 and CT453 are tunnel magnetoresistance (TMR) based, contactless, coreless, and differential current sensors. The only difference between the CT452 and CT453 is the operating voltage: CT452 operates from a 5 V supply, while CT453 operates from a 3.3 V supply; otherwise, the operating and electrical characteristics are identical. This application note references the CT452 and also applies to the CT453. These solutions are:

- **Contactless/Nonintrusive:** The sensor is placed over the current conductor [i.e., the printed circuit board (PCB) or the busbar].
- **Coreless:** Use of a magnetic concentrator/shield is not required.

- **Differential:** Features two internal TMR sensors able to measure a differential field and reject any common-mode external field.

The advent of electric vehicles and renewable energy has spearheaded the need for accurate and reliable current sensing in applications such as inverters for on-board AC-to-DC and DC-to-DC fast chargers, as well as high-voltage DC (HVDC) transmission systems. These and other high-current applications have demonstrated the need for cost-effective, high-accuracy current sensors capable of monitoring currents in the range of 50 A to greater than thousands of Amperes.

The CT452/3 is based on patented XtremeSense™ TMR technology, well suited for high-current applications. The sensor benefits from a high 1:4000 signal-to-noise ratio (SNR), as demonstrated with other Allegro TMR current sensors, allowing for resolutions in the hundreds of mA while measuring up to thousands of Amperes.

This application note introduces the concept of adding busbar slits for generating a localized differential magnetic field with a maximum coupling coefficient.

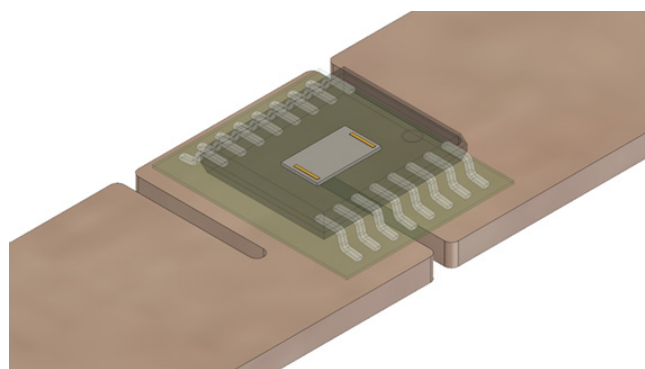


Figure 1: CT452/3 on Serpentine-Style Busbar

## OPERATING PRINCIPLE

The CT452/3 is a differential-magnetic-field sensor designed for high common-mode field-rejection capabilities. Two integrated TMR sensors are positioned in the package to detect a differential magnetic field generated by the three slits on the current-carrying busbar (Figure 1). The dual TMR sensors expect equal and opposite magnetic fields and, therefore, reject externally generated unidirectional fields.

Each TMR sensor is a full Wheatstone bridge with a 0.7 mm separation (Figure 2).

The CT452/3 also integrates signal-conditioning circuits that output the difference of the two TMR bridge outputs with a factory-trimmed gain setting:

Equation 1:  $V_{OUT}$  Equation

$$V_{OUT} = \text{Gain} \times (B_R - B_L),$$

where  $B_R$  and  $B_L$  are the right and left TMR sensor voltage outputs, respectively.

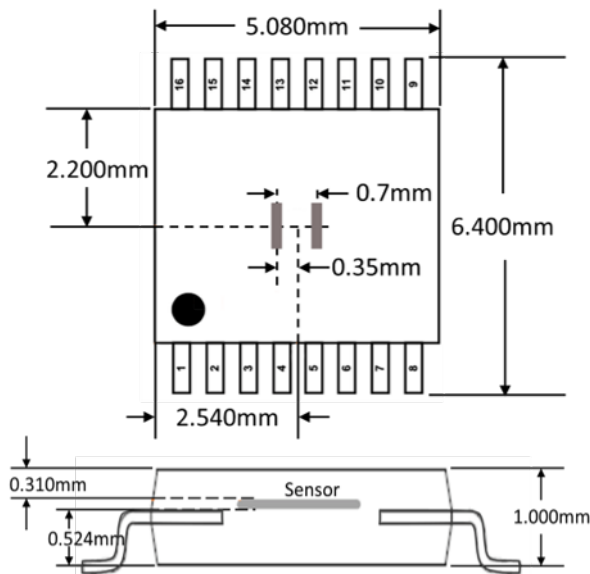


Figure 2: TMR Sense Element Positions

The  $V_{OUT}$  equation can be modified to include an external field,  $\epsilon$ , detected on both bridge sensors, as shown. With common-mode field rejection, this external field,  $\epsilon$ , is essentially cancelled as long as both TMR sensors detect the same external-field magnitude and direction:

$$V_{OUT} = \text{Gain} \times [(B_R + \epsilon) - (B_L + \epsilon)].$$

NOTE: If the busbar slit position is out of alignment with the 0.7 mm distance between TMR sensor bridges, magnetic fields generated by the primary current may not be detected identically. This leads to a reduction in the coupling coefficient, which reduces the gain of the current-sensing system. For an explanation of the impact of mechanical tolerances, refer to the Total System Accuracy section.

The current-carrying conductor (busbar or PCB trace) requires three slits to create a U-shaped current flow to generate a differential ( $B_L$  and  $B_R$ ) field, as shown in Figure 3.

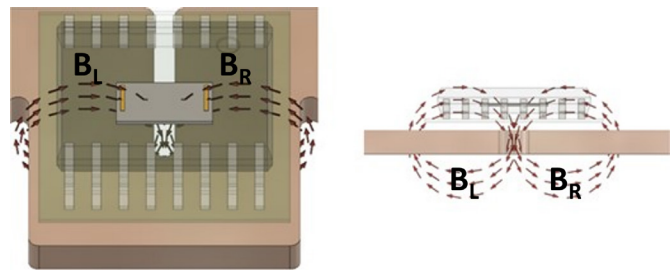


Figure 3: U-shaped Busbar, CT452/3, and Differential Magnetic Field Lines

## Busbar Design Guidelines

In practice, instead of designing a U-shaped busbar, it is easier to begin with a standard, rectangular, busbar then machine-in three slits to design the serpentine shape required for generating a differential field.

The key parameters of air gap (AG), slit width (W), slit length (L), slit height (H), busbar thickness (T), and busbar width (B) are identified in Figure 4 and Figure 5.

Simulation results for different busbar thickness, slit-height, and air-gap values are shown in Addendum A: COMSOL® Simulation Results. Each graph shows how the slit width and slit length impact the coupling coefficient. The busbar width is not a critical parameter for the coupling coefficient; therefore, Addendum A: COMSOL® Simulation Results assumes a busbar width of 12 mm. However, the slit height must be greater than half the busbar width.

Linear displacement and tilt impact the coupling coefficient, as shown for variable slit widths and lengths in Addendum B: Induced Percentage Error Change. To illustrate coupling coefficient losses, six axes of movement are evaluated: two axes of lateral displacement; one axis of vertical displacement (i.e., air gap); and three axes of tilt.

The graphs clearly indicate that, given all the dimensions, the best performance is achieved with minimal air gap.

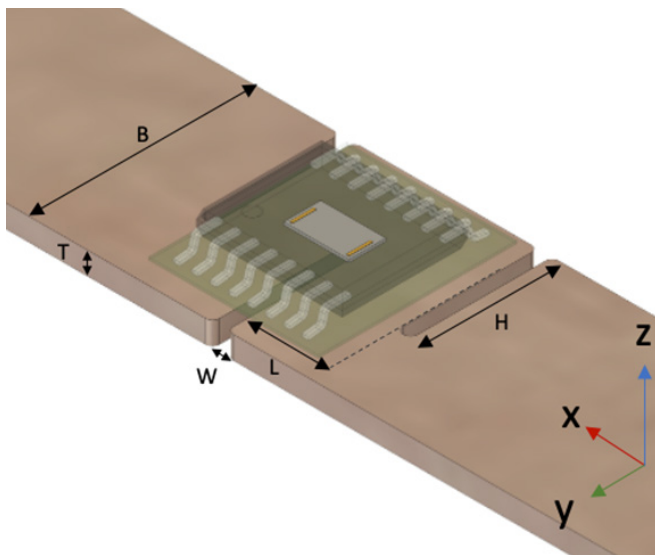


Figure 4: CTD452/3 on Serpentine-Shaped Busbar



Figure 5: Side-View of CTD452/3 on Top of Busbar

## EVALUATION BOARD BUSBAR EXAMPLE

The CTD452/3 evaluation board (see Figure 6) includes a copper busbar. The busbar has a current density of  $20 \text{ A/mm}^2$ , a cross-sectional width of 12.7 mm (B), and a thickness of 1.55 mm (T), for a current-carrying capability of up to  $\pm 400 \text{ A}$ .

With a busbar width of 12.7 mm (B), the absolute minimum slit height is  $12.7 \text{ mm} \div 2 = 6.35 \text{ mm}$ . The final selected slit size is 7.35 mm, which provides a 1 mm margin to facilitate mechanical displacement along the Y-axis. The slit-height dimension must be larger than half the busbar width.

The coupling coefficient based on the above parameters is  $3.9 \mu\text{T/A}$ , which—using the CT452-H06MRTS16 with a bipolar-magnetic-field detection of  $\pm 6 \text{ mT}$  and a sensitivity of  $333.3 \text{ mV/mT}$ —generates a  $V_{\text{OUT}}$  signal of  $1.3 \text{ mV/A}$  ( $333.3 \text{ mV/1000 } \mu\text{T} \times 3.9 \mu\text{T}$ ).

The total dynamic range of the sensor is  $\pm 1500 \text{ A}$ . The resolution of this system is slightly better than 1 A because the noise of the sensor over 100 kHz bandwidth (BW) is rated at  $2.77 \mu\text{T}$ .

In this example, the busbar is placed under the PCB. Hence, the distance between the TMR sense elements and the busbar is the PCB thickness of 1.55 mm plus 1.05 mm to the top of the package. The die is 0.3 mm from the top of the package; the final position is then 2.3 mm.

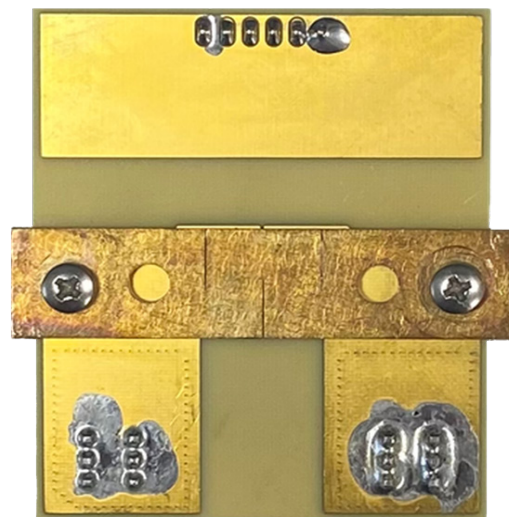


Figure 6: CTD452/3 with Busbar Mounted on Bottom

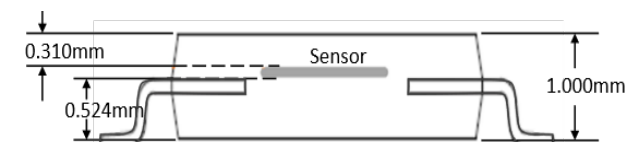


Figure 7: TMR Sensor Element Position Inside Package

## TOTAL SYSTEM ACCURACY

Three factors impact total system accuracy:

- CT452/3 sensor accuracy
- Mechanical tolerances
- Busbar design

Every CT452/3 is factory trimmed and calibrated. For gain, offset, and linearity error specifications along with their drift specifications over temperature and lifetime, refer to the electrical characteristics provided in the datasheet.

Busbar manufacturing tolerances are typically small and do not represent a source of error when calculating total system error. However, mechanical tolerances do contribute to the coupling coefficient, which impacts the overall gain of the system.

Mechanical tolerances can be categorized as either:

- Mounting mechanical tolerances, which occur due to manufacturing tolerances; or
- Lifetime mechanical tolerances, which occur due to vibrations and thermal stress.

For the best total system accuracy, performance of end-of-line system calibration is recommended (instead of focusing on reducing manufacturing tolerances).

### Thermal Considerations

The main limiting factor when designing with serpentine slits is the temperature rise of the current-carrying conductor. Any busbar design should begin with a thermal definition of the system to understand its limitations. This includes materials used, system cooling, heat sources or sinks, current on-time, and current density.

A thermal image of the evaluation board serpentine busbar under  $300 A_{DC}$  is shown in Figure 8. The increased temperature is found at the busbar terminal connections due to the increased resistance of the cable size and terminal bonding. However, the measured thermal rise at the busbar center, where the CT452/3 current sensor would be located, is approximately  $70^{\circ}C$ .

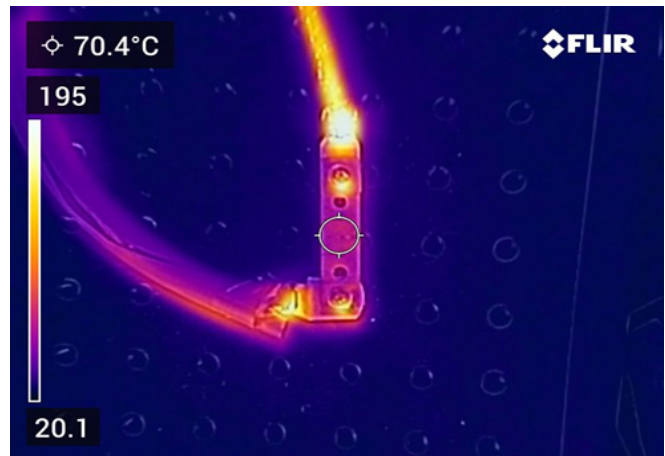


Figure 8: Evaluation Board Thermal Image at  $300 A_{DC}$

## CONCLUSION

The CT452/3 is a contactless, coreless, differential current sensor based on XtremeSense TMR technology from Allegro. It can achieve sub-1 A resolution with a dynamic range of  $\pm 100 A$  to  $\pm 1000s$  of Amperes.

The air-gap between the sensor and the busbar is the single-most important parameter to optimize in a serpentine busbar design. The next most-critical parameter is the slit width/length.

The CT452/3 offers a novel approach to current sensing with high SNR and common-mode field rejection. For more information, visit [allegromicro.com](http://allegromicro.com).

## ADDENDUM A: COMSOL® SIMULATION RESULTS

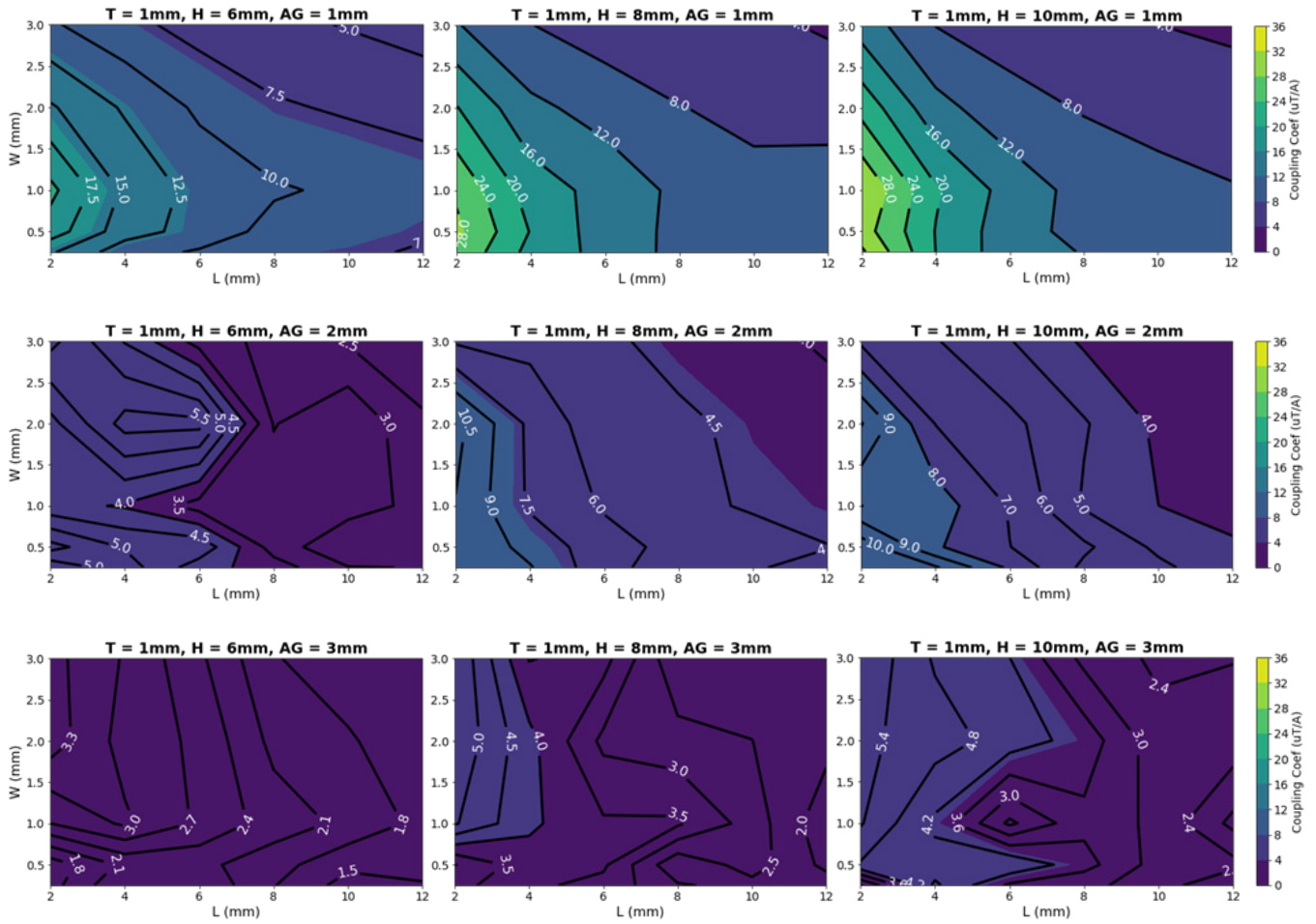


Figure 9: Coupling Factor with Busbar Thickness of 1 mm

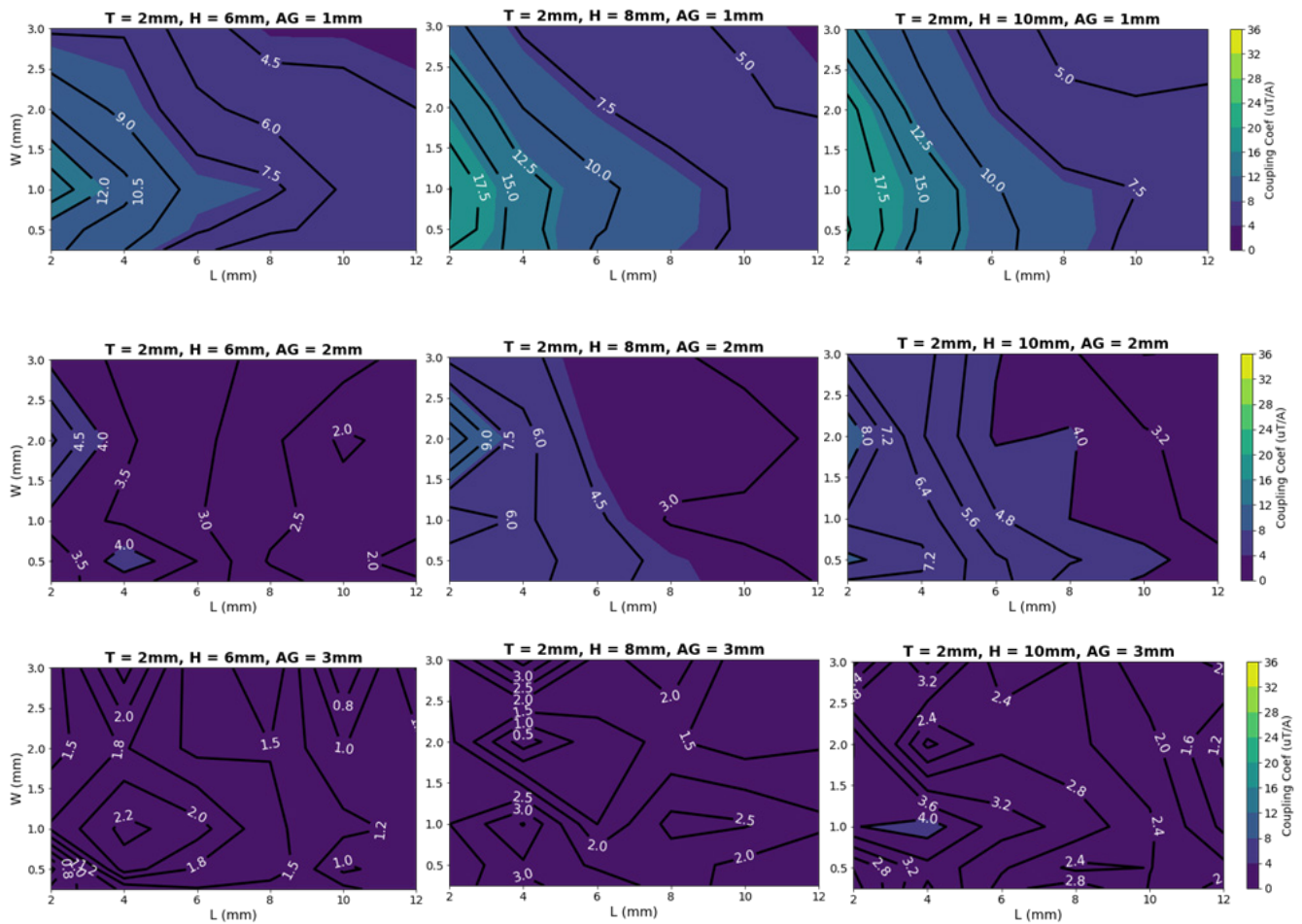


Figure 10: Coupling Factor With Busbar Thickness of 2 mm

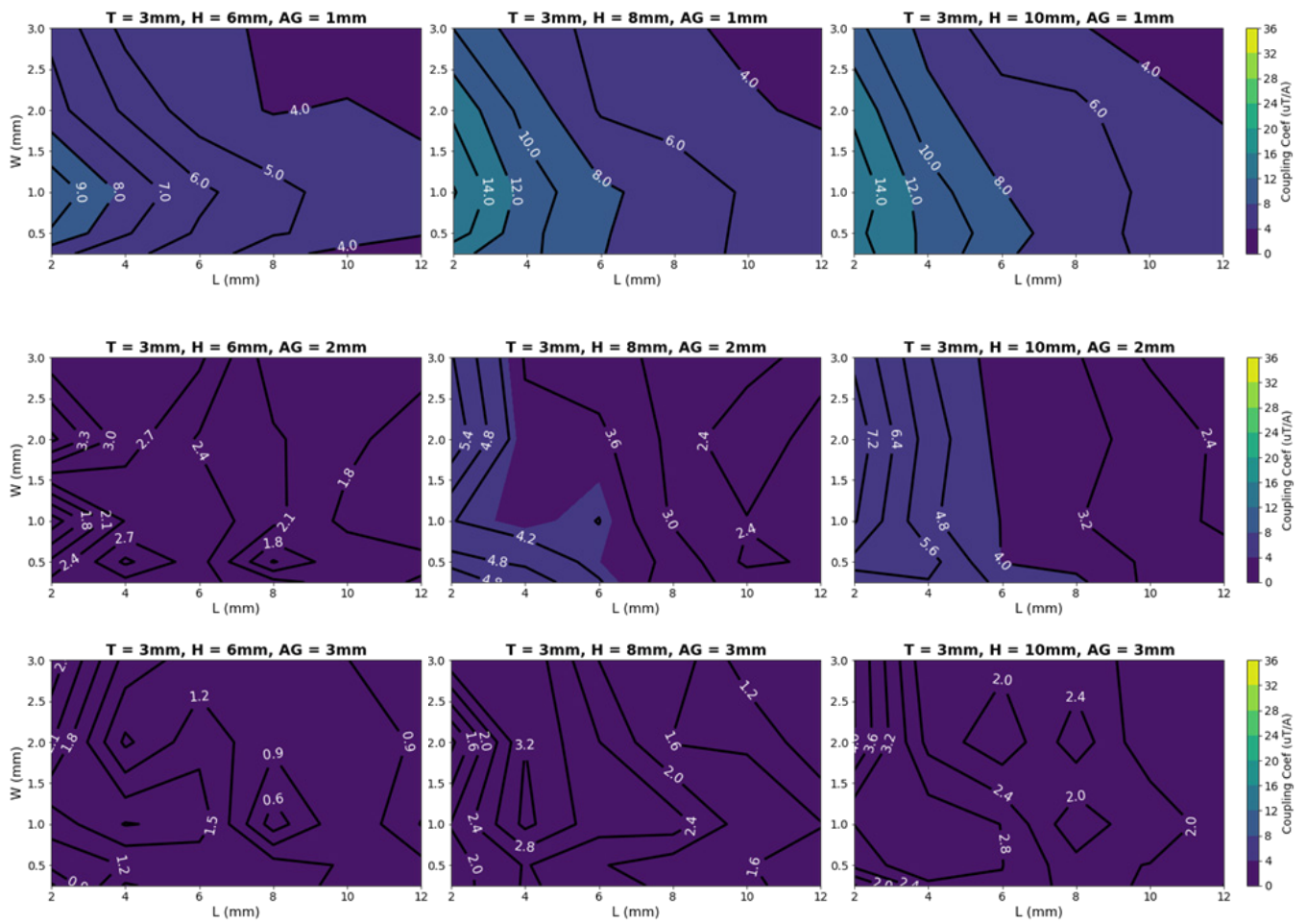


Figure 11: Coupling Factor with Busbar Thickness of 3 mm

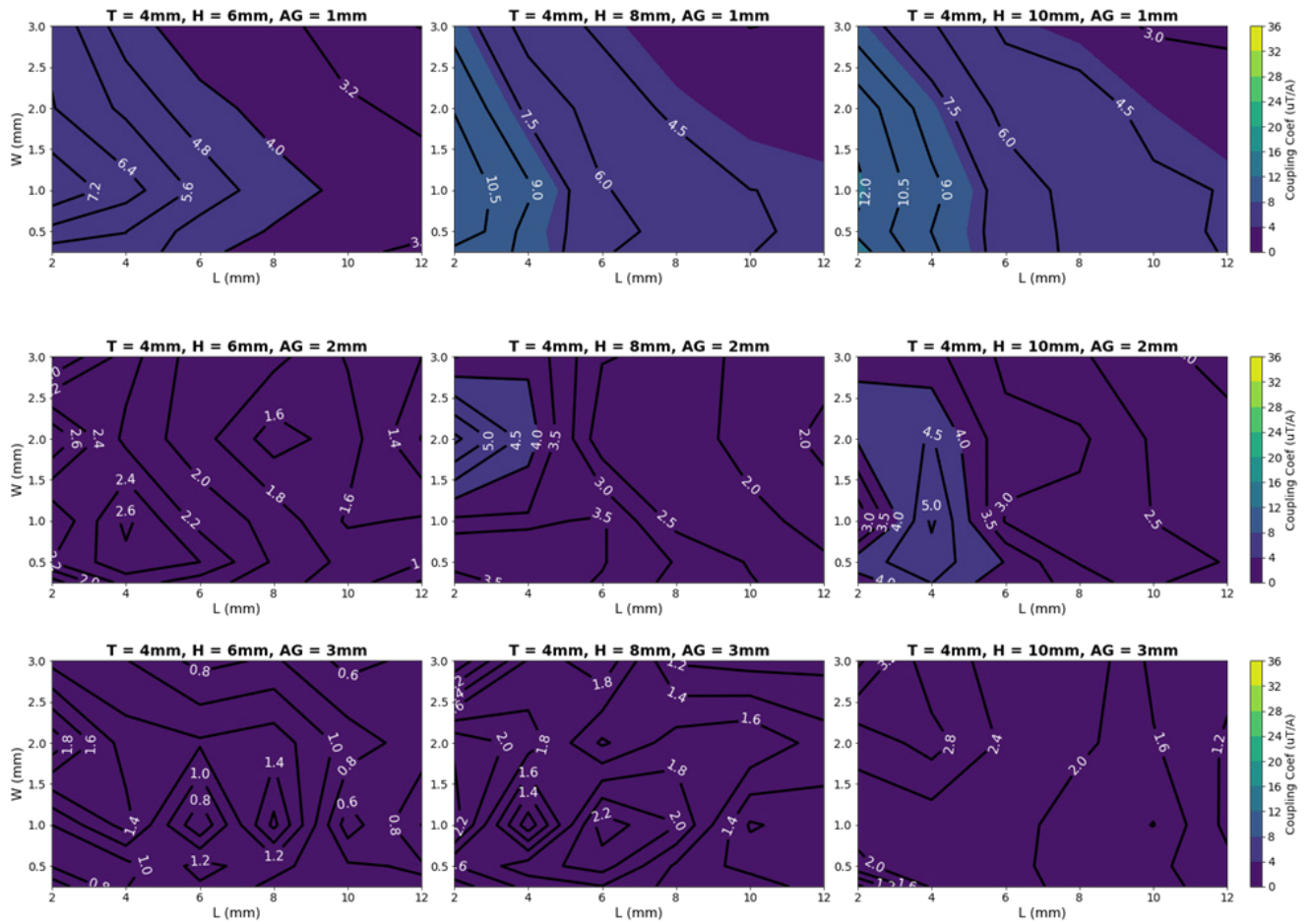


Figure 12: Coupling Factor with Busbar Thickness of 4 mm



## ADDENDUM B: INDUCED PERCENTAGE ERROR CHANGE

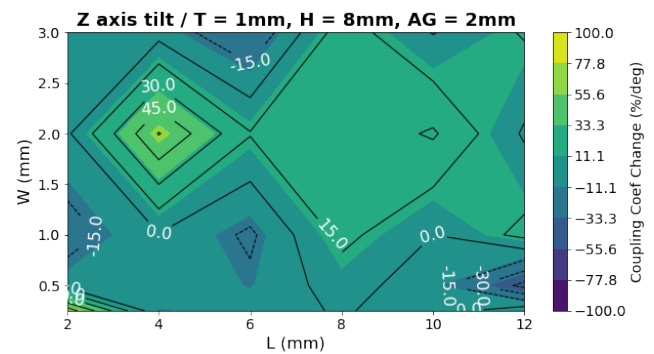
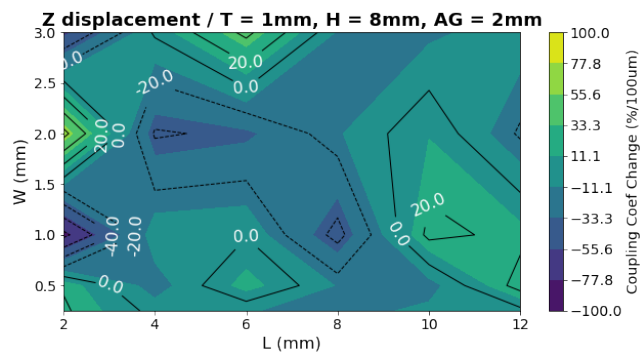
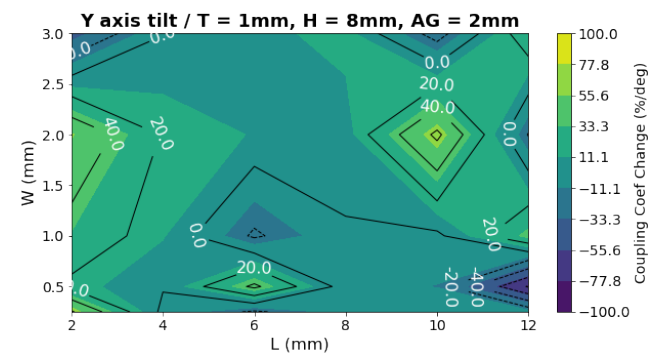
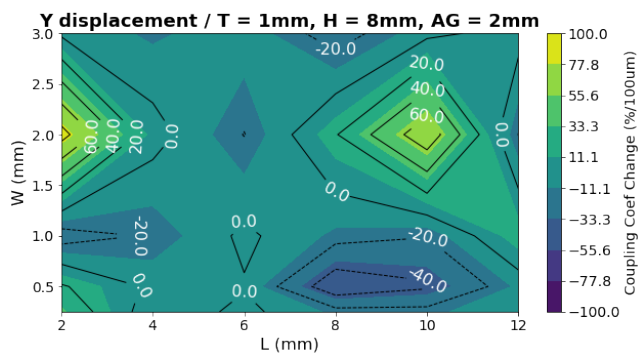
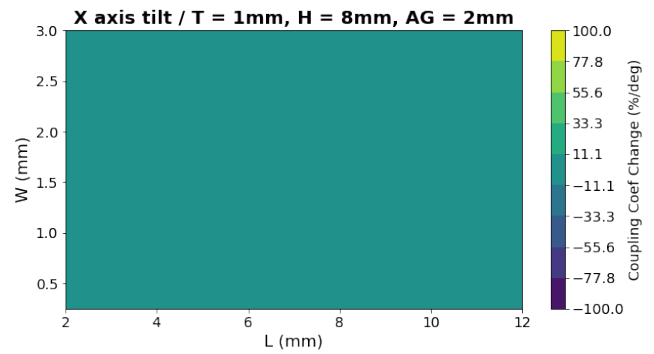
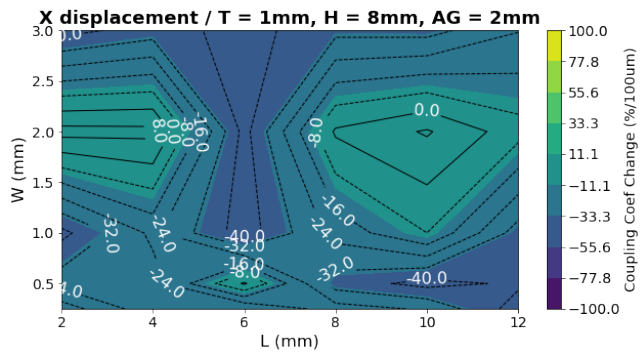


Figure 13: Mechanical Displacement-Induced Percentage Error Change

Figure 14: Mechanical Tilt-Induced Percentage Error Change

*Revision History*

Number	Date	Description	Responsibility
1	November 30, 2023	Document rebrand and minor editorial corrections	J. Henry

Copyright 2023, Allegro MicroSystems.

The information contained in this document does not constitute any representation, warranty, assurance, guaranty, or inducement by Allegro to the customer with respect to the subject matter of this document. The information being provided does not guarantee that a process based on this information will be reliable, or that Allegro has explored all of the possible failure modes. It is the customer's responsibility to do sufficient qualification testing of the final product to ensure that it is reliable and meets all design requirements.

Copies of this document are considered uncontrolled documents.